Inertial particles in homogeneous shear turbulence

Journal of Physics: Conference Series **318** (2011) 052009 doi:10.1088/1742-6596/318/5/052009

Inertial particles in homogeneous shear turbulence

Claudia Nicolai[1,2], Boris Jacob[1], Paolo Gualtieri[2] and Renzo Piva[2]

[1] CNR-INSEAN, via di Vallerano 139, 00128 Rome, Italy

[2] DMA, Sapienza Università di Roma, Via Eudossiana 18, 00184 Rome, Italy

E-mail: claudia.nicolai@uniroma1.it

Abstract. The characteristics of inertial particles distribution in a uniformly sheared turbulent flow are investigated, with the aim of quantifying the effects associated with the large-scale anisotropy induced by the mean velocity gradient. The focus of the analysis is on clustering aspects, and in particular on the dependence of the radial distribution function on both the directionality and the magnitude of the observation scale. We discuss experimental data measured in a homogeneous shear flow seeded with particles of size comparable with the Kolmogorov length scale and Stokes number $St \approx 0.3$, and discuss their distribution properties in comparison with results provided by related one-way coupled direct numerical simulations which make use of the point-force approximation.

1. Introduction

Two-phase particle-laden turbulent flows are central to a wide spectrum of engineering applications (e.g. those relying on atomization or spray-injection processes) as well as to numerous natural phenomena, ranging from the dispersion of pollutants in the atmosphere to plankton transport in the oceans. Understanding the main features of the interaction between the carrier velocity field and the dispersed phase, as an essential prerequisite for optimizing industrial processes or predicting environmental issues, has therefore been the subject of numerous experimental and computational studies in the last decades, see e.g. the recent review (Balachandar & Eaton, 2010) and references therein.

For dilute flows at low value of the particle concentration, no substantial modification of the underlying flow field is expected to be introduced by the presence of the dispersed phase. The interest in this *one-way coupling* régime stays in the study of particle transport by the turbulent field in terms e.g. of the particle mean square displacement, a process which is mainly controlled by large-scale eddies. More recently, attention has been directed also to small scale aspects, and in particular to the phenomenon of preferential accumulation (Squires & Eaton, 1991; Wang & Maxey, 1993), namely the strong instantaneous non-uniformities of the concentration field which are due to differences in the inertia of the two phases. Actually, finite-size particles do not sample the fluid domain uniformly under the action of turbulent diffusion but tend to collect in certain regions of the flow. Small heavy particles are observed to be ejected from high-vorticity zones and cluster in regions of high strain. Lighter-than-fluid particles display the opposite tendency and migrate towards high-vorticity regions. The resulting patchiness which characterizes the instantaneous concentration field is of particular interest since it may affect important processes such as the rate of inter-particle collisions or bubble coalescence. Many investigations suggest that the phenomenon seems to be controlled by the smaller scales of the

flow, since the effects associated with the inhomogeneities are usually found to be amplified when the particle relaxation time approximately matches the Kolmogorov time scale (see e.g. Balachandar & Eaton, 2010).

At increasing particle volume fractions or mass loads, the back-reaction of the particles on the turbulent field may significantly alter the flow evolution. The transition towards this *two-way coupling* régime is usually identified when the particle volume fraction $\overline{C}$ is of the order of 10^{-6} (Balachandar & Eaton, 2010). Interestingly, even at such modest values of the volume fraction, large concentration overshoots are created by the mechanism of inertial clustering, and the strong localized feedback on the carrier velocity field can ultimately lead to profound modifications of the turbulence structure even at larger scales, see e.g. (Jacob *et al.*, 2010) for the case of a bubble-laden turbulent boundary layer. Modifications of other important integral quantities such as energy dissipation, overall turbulent intensity or particle setting have been reported for various flow configurations (e.g., Tanaka & Eaton, 2008).

To characterize the features of both the one- and the two-way coupling interaction, the effects of particle inertia (determined by particle size and solid-to-fluid density ratio), volume fraction and other control quantities such as gravity, turbulence characteristics or mean shear should be separately and systematically examined. In principle, the numerical approach is suitable for such a parametric investigation. However, direct numerical simulations are usually forced to drastic simplifications to make computations affordable. In fact, fully resolved computations with realistic numbers of finite-size particles have been obtained only recently for the case of isotropic turbulence (Lucci *et al.*, 2010). Most studies on jets, channels, homogeneously sheared- and isotropic flows have been carried out instead in the context of the so-called point-force approximation (see an up-to-date list in e.g. Eaton, 2009), i.e. they are focussed on the transport of heavy sub-Kolmogorov particles for which a minimal description in terms of material points advected by suitably parametrized forces (e.g., a Stokes drag) proves sufficiently accurate. On the other hand, isolating the effects of the different control parameters from an experimental point of view is hampered by a number of reasons, e.g. the difficulties associated with optical measurements in two-phase flows or the impossibility of changing the single governing quantities independently. In fact, the valuable results collected for the cases of isotropic or wall-bounded turbulence (Poelma *et al.*, 2007; Aliseda *et al.*, 2002; Tsuji *et al.*, 1984; Kiger & Pan, 2002) as well as for jets and mixing layers (Longmire & Eaton, 1992) are typically restricted to a limited range of control parameters, which only rarely overlaps with the corresponding numerical data.

In the present paper, we wish to contribute to the understanding of *dilute* two-phase flows by exploring the influence of a mean velocity gradient on the distribution of inertial particles. Data are obtained both from numerical simulations and laboratory measurements in a novel and specifically designed experiment. The flow under investigation is a homogeneous shear flow, which is characterized by almost uniform values of the mean shear and turbulent intensity. It thus retains the distinctive feature of common turbulent flows such as boundary layers or jets, yet the absence of solid boundaries or spatial inhomogeneities allows a drastic simplification of the analysis. For instance, complications involving the well-known turbophoresis effect, i.e. the particle flux in the direction of turbulent intensity gradients, are excluded. In this paper, we intend to focus on the small-scale features of the concentration field to study the clustering phenomenon. In this context, one of the main purposes is to assess the capabilities of the numerical approach to qualitatively reproduce the salient features observed in the laboratory. Experimental results concerning the velocity statistics of both the carrier flow and the particles will be reported in a future paper.

2. Experimental dataset

2.1. The homogeneous shear flow

The experiment is conducted in a closed-loop, free-surface water tunnel with a cross-sectional area of $0.6 \times 1\,m^2$ and a $25\,m$ long test section Water is circulated by means of 3x20 kW pumps which allow to reach a maximum velocity approximately equal to $1\,m/s$.

The uniformly sheared turbulent flow is generated by means of a grid with uniform mesh, whose profile is suitably shaped following the original idea and the design rules described in (Dunn & Tavoularis, 2007). Compared to the classical technique, which uses a series of parallel channels with different solidities tuned after a trial-and-error procedure, this solution allows a much faster implementation in a water facility. The drawback is represented by the necessity of constructing a new screen whenever the intensity of the mean shear S needs a substantial modification. A sketch of the experimental apparatus, together with the definition of the coordinate system, is given in the left panel of Fig. 1.

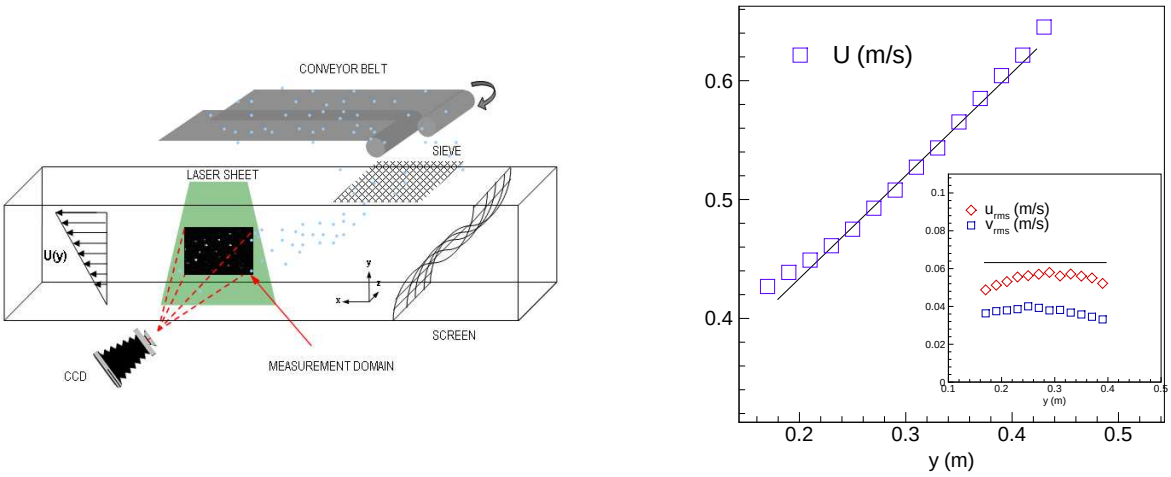

Figure 1. Left panel: sketch of the experimental setup. Right panel: the mean velocity U as a function of vertical coordinate y. The inset shows the streamwise and vertical velocity fluctuation profiles.

In order to check the quality and the evolution of the flow field, we have measured the velocity profiles at different distances downstream of the generating screen by means of a two-component Laser Doppler anemometer powered by a $6\,W$ Argon-Ion continuous laser. Note that the data rate of each velocity signal was sufficient to ensure a resolution at the level of the Kolmogorov time-scale τ_η, and to obtain one-dimensional estimates of the energy dissipation rate ϵ by time differentiation and use of Taylor hypothesis. Typically, at least 10^6 data points were acquired at each measurement location to obtain convergence of second-order statistics.

The behavior of the turbulent profiles measured at a downstream distance $x = 4\,m$ is given in the right panel of Fig. 1. An almost linear variation in the vertical direction is observed for the mean velocity U over a substantial portion of the measuring section. At the same time, profiles of both the streamwise and the vertical velocity fluctuation display good uniformity over the same spatial region, in compliance with the requirements of a homogeneous shear flow. Flow statistics are known to exhibit a slow evolution with downstream distance. In our case, marginal variations of the mean velocity profile, of the order of a few percent, were observed over a distance of $3\,m$. The relevant turbulent quantities at $x = 4\,m$ are summarized in Table 1. In particular, the two parameters which are usually characterize this kind of flow, namely the

Reynolds number $Re_\lambda = \lambda\, u_{rms}/\nu$ and the shear parameter S^* representative of the extension of the interval of turbulent scales whose velocity statistics are affected by the large-scale anisotropy ($S^* = Su^2_{rms}/\epsilon$) are respectively equal to $Re_\lambda \approx 530$ and $S^* \approx 4.5$.

Table 1. Relevant properties of the homogeneous shear flow and of the inertial particles.

U_c $[\frac{m}{s}]$	L $[m]$	η $[mm]$	u_{rms} $[\frac{m}{s}]$	v_{rms} $[\frac{m}{s}]$	$\rho_{\overline{uv}}$	Re_λ	S^*	$\overline{d}$ $[mm]$	ρ_p/ρ_f	v_t/u_{rms}	St	$\overline{C}$
0.52	0.15	0.2	0.06	0.04	-0.34	530	4.5	0.25	2.6	0.6	0.28	10^{-6}

2.2. Particle seeding and identification

In order to seed the flow in a continuous and uniform way, a given amount of solid-phase particles is first homogeneously distributed over a $5\,m$ long conveyor belt, and then released into the water after passing through a series of sieves positioned immediately above the free surface (see Fig. 1). A continuous cloud of particles is thus generated, whose width in the $y-$direction at the measurement station can be adjusted by modifying the streamwise extent of the area over which particles are distributed. Particle concentration is controlled by the conveyor speed.

In this paper we focus on the particular case of approximately mono-disperse glass beads with mean diameter $\overline{d} \simeq 0.25\,mm$ and density ratio $\rho_p/\rho_f \simeq 2.6$ ($\rho_f = 1000\,kg^{-3}$). Note that such particles are only slightly larger than the local Kolmogorov lengthscale ($\overline{d}/\eta \simeq 1.25$), and the Stokes number based on mean diameter, i.e. the ratio between the particle relaxation time $\tau_p \approx 0.01\,s$ and the Kolmogorov time-scale $\tau_\eta \approx 0.036s$ is $St \simeq 0.28$. The dispersion of the particle diameter histogram amounts to $\sigma_d \approx 20\,\mu m$. The typical ensemble-averaged concentration at the measurement location is $\overline{C} \approx 10^{-6}$ and the mass loading $\overline{m} = \rho_p/\rho_f\,\overline{C}$ is $\overline{m} \approx 2.6\,10^{-6}$, which are sufficiently low to safely ignore two-way coupling effects.

Concerning particle identification, a laser light sheet in the vertical (xy) plane is used in conjunction with a 2848 × 4288 pixel CCD camera equipped with a 105 mm lens in order to

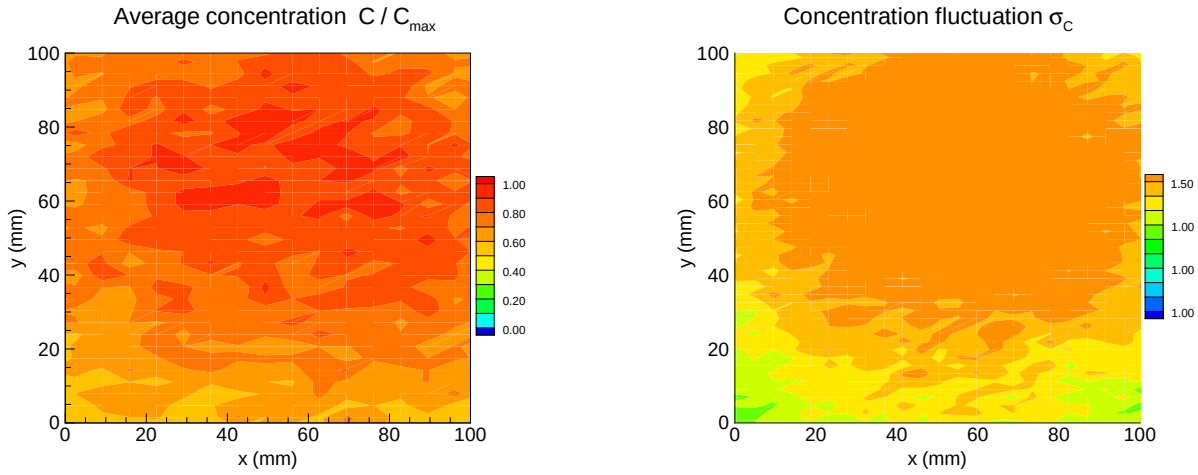

Figure 2. Left panel: spatial variation of the local ensemble-averaged particle concentration C, normalized with its peak value. Right panel: spatial variation of the root-mean-squared value σ_C of the local particle concentration.

acquire the instantaneous position of particles within a measurement domain approximately equal to $80 \times 100\, mm^2$. Particle centroids are obtained with sub-pixel accuracy by processing the digital frames with standard procedures involving a sequence of high- and low-pass filtering operations (Crocker & Grier, 1996). It is important to note that the flow region where particles are dispersed is sufficiently extended to legitimate the assumption that the particle distribution is statistically homogeneous. This can be appreciated in the left panel of Fig. 2, where the local particle concentration (averaged over an ensemble of 1000 frames) is displayed as a function of the spatial coordinates. No significant large-scale inhomogeneities are evident over spatial lengths which are comparable with the integral scale L of the turbulence. Note in particular that the variation of the coarse grained concentration is less than 10% in the domain where the characterization of the particle distribution will be performed, namely the central area of size $20 \times 20\ \ mm^2$. This holds also for second- and fourth-order statistics, as illustrated by the satisfactory spatial uniformity observed for the variance of the local concentration in the right panel of Fig. 2.

3. Numerical dataset

The technique described in Rogallo (1981) is employed to write the Navier-Stokes equations for the velocity fluctuations $\mathbf{u}$ in a deforming coordinate system convected by the mean flow according to the transformation of variables $\xi_1 = x - Sty; \quad \xi_2 = y; \quad \xi_3 = z; \quad \tau = t$. The resulting system

$$\nabla \cdot \mathbf{u} = 0\,; \qquad \frac{\partial \mathbf{u}}{\partial \tau} = (\mathbf{u} \times \boldsymbol{\zeta}) - \nabla \pi + \nu \nabla^2 \mathbf{u} - S u_2 \mathbf{e}_1 + \mathbf{F}\,,$$

is numerically integrated by a pseudo-spectral method combined with a fourth order Runge-Kutta scheme for temporal evolution, see (Gualtieri *et al.*, 2002). In the above system of equations, $\boldsymbol{\zeta}$ is the curl of $\mathbf{u}$, π is the modified pressure which includes the fluctuating kinetic energy $|\mathbf{u}|^2/2$, ν is the kinematic viscosity. The Navier-Stokes equations are integrated in a $4\pi \times 2\pi \times 2\pi$ periodic box with a resolution of $256 \times 256 \times 128$ Fourier modes, corresponding to $384 \times 384 \times 192$ collocation points in physical space due to the 3/2 dealiasing rule. The Kolmogorov scale is $\eta = 0.02$, corresponding to $K_{max}\eta = 3.1$. This ensures sufficient resolution at small scales.

The two parameters controlling the homogeneous shear flow, the Taylor-Reynolds number $\mathrm{Re}_\lambda = \sqrt{5/(\nu\epsilon)}\langle u_\alpha u_\alpha \rangle$ and the shear strength $S^* = S\langle u_\alpha u_\alpha \rangle/\epsilon$, are respectively equal to $\mathrm{Re}_\lambda \simeq 100$ and $S^* \simeq 7$, corresponding to a ratio of shear to Kolmogorov scale $L_s/\eta \simeq 35$. The dispersed phase consists of point-like spherical particles with diameter d_p much smaller than the Kolmogorov scale and with mass density ρ_p much larger than the carrier fluid ρ_f. It follows that the only relevant force is the Stokes drag (Maxey & Riley, 1983). Accordingly, the equations for particles position $x_i^p(t)$ and velocity $v_i^p(t)$ are $\dot{x}_i^p = v_i^p\,; \quad \dot{v}_i^p = f_i^p$ where $v_i(x^p, t)$ is the instantaneous fluid velocity evaluated at the particle position $x_i^p(t)$, $f_i^p = \tau_p^{-1}\left[v_i(x^p, t) - v_i^p(t)\right]$ is the Stokes drag, $\tau_p = \rho_p d_p^2/(18\nu\rho_f)$ is the Stokes relaxation time. The particle equations are integrated by the same fourth order Runge-Kutta scheme used for the Navier-Stokes equations, with fluid velocity at particle positions evaluated by tri-linear interpolation. Actually a well-resolved velocity field is crucial to minimize numerical errors associated with the interpolation which is necessary to advect the particles in the present mixed Eulerian-Lagrangian formulation, see (Gualtieri *et al.*, 2009) for more details and references.

Starting from an already fully developed fluid velocity field in statistically steady conditions, five different populations of $N_p = 300000$ particles each, with Stokes numbers $St_\eta = 0.1, 0.5, 1.0, 5.0, 10.0$, are initialized with random and homogeneous positions and velocities matching that of the local fluid. Samples for particle statistics corresponding to 480 independent

snapshots separated in time by $2\,S^{-1}$ are collected after an initial transient of $50\,S^{-1}$. Discarding the initial transient is crucial to have results independent from the rather arbitrary initial state used to initialize the particles.

4. Characteristics of the particle distribution

A first impression concerning the features of the particle distribution can be gained from the plots in Fig. 3, which show the positions of inertial particles in a vertical $(x-y)$ thin sheet for both the experimental and the numerical datasets. The patchiness of the distribution, as well as the tendency of particles to cluster in thin elongated structures with a preferential orientation in the direction of the maximum mean strain rate, is apparent. This aspect is particularly accentuated for the numerical dataset at $St = 1$, and the analysis of the vorticity field confirms that the regions devoid of particles separating the clustering areas are indeed characterized by large values of the enstrophy (Squires & Eaton, 1991).

In order to provide a statistical description of these aspects, a number of tools have been developed in the literature. Typically, one aims at quantifying the effects of preferential accumulation at a given lengthscale r by defining appropriate measures representative of the deviation from a purely random distribution of particles, as described by Poissonian statistics (e.g., Wang & Maxey, 1993; Eaton & Fessler, 1994). For the case of isotropic turbulence, a commonly used indicator is the so-called radial distribution function $g(r)$, which compares the probability of finding two particles at separation distance r with the probability of finding them at the same distance in the pure random case. Operatively, for a two-dimensional situation such as the one depicted in Fig. 3, the radial distribution function is computed from the coordinates of the particles as:

$$g(r) = \frac{N(r)/\Delta S(r)}{N/A},$$

where $N(r)$ represents the number of particles found in a circular shell of thickness Δr and radius r centered on the generic base particle, N/A represents the density of possible particle pairs in the measurement domain A, and an ensemble-average is performed over the set of snapshots. Deviation of $g(r)$ from a unit value indicates non-Poisson behavior of the particle distribution

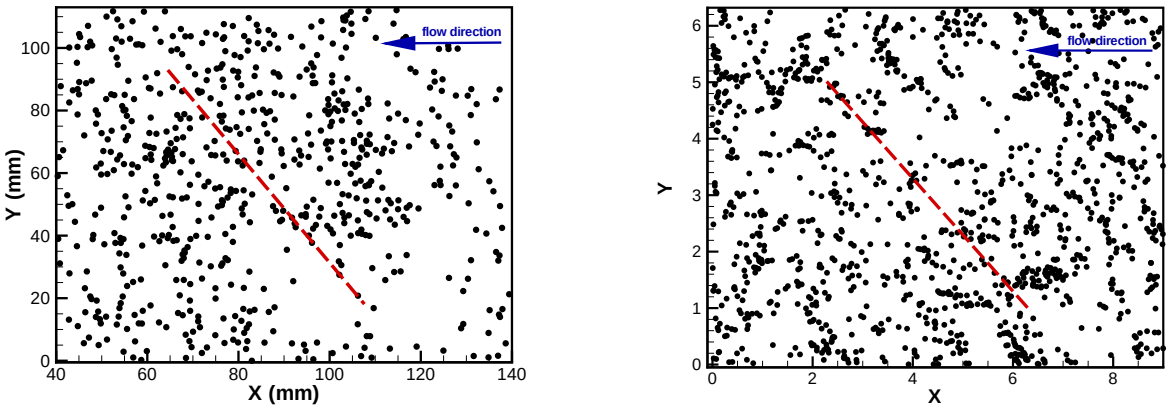

Figure 3. Spatial distribution of the inertial particles. Left panel: experimental data ($St = 0.3$). Right panel: numerical data ($St = 0.5$). The dashed line indicates the direction of the maximum mean strain rate.

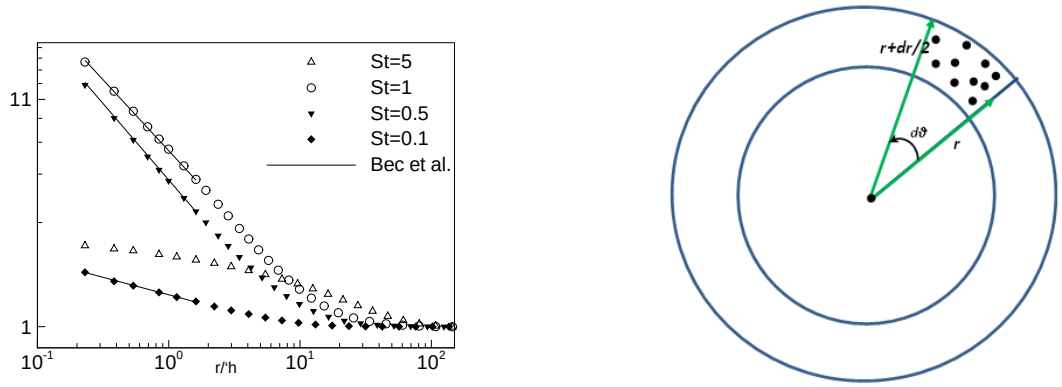

Figure 4. Left panel: the circular average of $\widetilde{g}(r,\theta)$ as a function of the separation scale r for DNS data at different values of the Stokes number. Right panel: definition of the angular distribution function $\widetilde{g}(r,\theta)$.

at that given scale. Namely, preferential particle accumulation is associated with the strong increase of $g(r)$ which is commonly observed at small scales. This effect depends on the value of the Stokes number, and is usually found to be amplified when $St = 1$, as illustrated in the right panel of Fig. 4 for the DNS data (note that a suitable spherical averaged has been performed in order to remove the directional dependence). Theoretical arguments can be used for point-like heavy particles to predict power-law behaviour in the form $g(r) \sim r^{\alpha}$ at small separations (Bec *et al.*, 2007).

The extension to situations where the isotropy constraint breaks down, such as in presence of a large-scale anisotropy induced by a mean shear, is readily achieved by taking the directionality of the statistics into account. Namely, we can introduce a new indicator $\widetilde{g}(r,\theta)$, depending on both the magnitude r and the direction θ of the separation vector $\mathbf{r}$, with which we gauge the probability of detecting a particle in an area element $rd\theta dr$ located at distance $\mathbf{r}$ away from a test particle (as illustrated in the right panel of Fig. 4), and compare it with the case of a uniform distribution. The function $\widetilde{g}(r,\theta)$ has been computed for the experimental and the

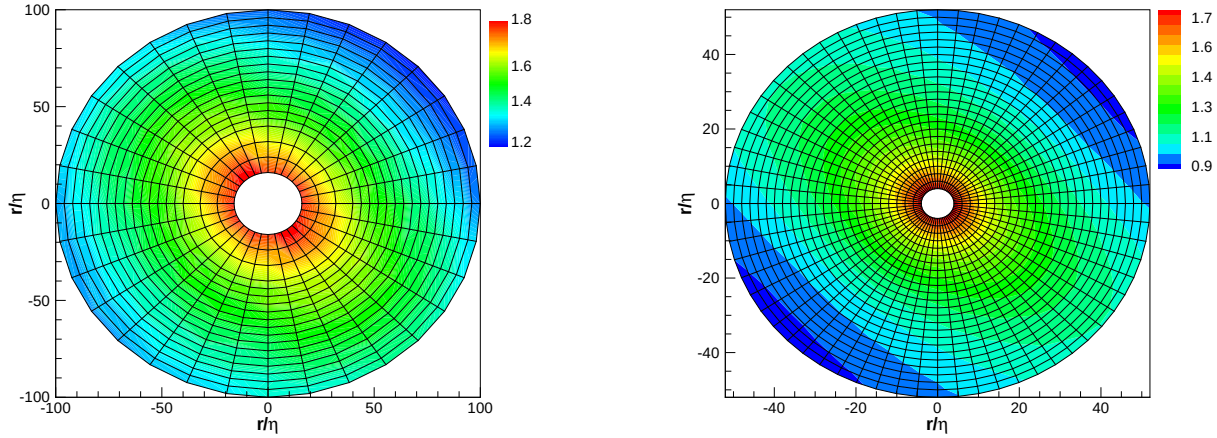

Figure 5. Left and right panels: the distribution function $\widetilde{g}(r,\theta)$ computed for the experimental data and for the numerical case at $St = 0.5$, respectively.

numerical data ($St = 0.5$), and is shown in Fig. 5. At a first glance, the qualitative agreement between the two situations may appear satisfactory. However, it is clear that, in view of the simplifications adopted in the DNS for the description of particle motions, the comparison requires some caution. In fact, we cannot naively expect a quantitative agreement between numerical data and experimental results at corresponding values of the Stokes number, since relevant aspects such as those associated with finite-size effects or gravity are not taken into account by the numerics. Other parameters come also into play. In particular, the effects of the Reynolds number Re_λ and of the shear parameter S^*, which are the quantities fixing the range of eddies able to interact with a given class of particles (Casciola *et al.*, 2007; Yoshimoto & Goto, 2007), need to be taken into a due consideration. Despite the apparent mismatch, the main features observed in the experiment seem to be qualitatively reproduced in the simulations. As it appears from Fig. 5, the preferential accumulation manifests itself with the increase of $\widetilde{g}$ observed at decreasing scale for given direction of the separation vector $\mathbf{r}$. The anisotropy of the carrier field is reflected in the particle distribution through the marked variation of $\widetilde{g}$ with angle θ for fixed separation scale r. Consistently with the preferential particle patterns observed in Fig. 3, sharp maxima are observed at $\theta \approx 45^\circ$, i.e. in the direction of the maximum mean strain.

It is of course of fundamental importance to try to link the properties of the particle distribution to those of the carrier velocity field, and in particular to assess whether the large-scale anisotropy of the particle patterns tends to vanish as the separation scale is reduced, as is the case for the velocity field (Casciola *et al.*, 2007). Proper tools which rigorously characterize the particle field anisotropy at changing scale r can be constructed based on $SO(3)$ decomposition techniques, i.e. a statistical observable is decomposed in terms of spherical harmonics with scale-dependent coefficients (Biferale & Procaccia, 2005). For two-dimensional data, we make use of the $SO(2)$ decomposition in order to express the function $\widetilde{g}(r,\theta)$ in terms of separation distance r and direction θ as:

$$\widetilde{g}(r,\theta) = \sum_n c_n(r) e^{jn\theta}.$$

In this framework, we associate increasing levels of anisotropy to increasing values of the index n which labels the different Fourier harmonics. An example of such a decomposition for the experimental dataset (left panel of Fig. 6) shows that the most energetic anisotropic mode, i.e. the largest contributor to the angular modulation of $\widetilde{g}(r,\theta)$, corresponds to $n = 2$. In order to quantify the amount of anisotropy found in the particle distribution at a given scale r in the present case, it is therefore natural to introduce an anisotropic indicator as the ratio between the amplitudes of the second mode and that of $n = 0$, i.e. the mean value of $\widetilde{g}(r,\theta)$. The anisotropy indicator $I_A(r)$ is thus estimated as: $I_A(r) = c_2(r)/c_0(r)$, and its variation when the separation distance r/η spans the interval $[10 \div 60]$ is reported in the right panel of Fig. 6 for the experimental as well as for numerical datasets. Note that, in the experiment, a significant isotropization of the particle distribution is found to occur, i.e. patches of particles tend to become isotropic as their size is reduced to sufficiently small values. No such effect is observed in numerical simulations of point-like particles at corresponding values of the Stokes number (i.e., $St = 0.5$), where on the contrary clustering anisotropy keeps increasing as the scale gets finer, and eventually saturates once the Kolmogorov scale is reached (Gualtieri *et al.*, 2009).

As mentioned before, we believe that such differences should be reconsidered in the light of the different values of the Reynolds number and shear intensity achieved in the DNS and in the experiments. In fact, as the Taylor Reynolds number in the DNS turns out to be about five times smaller compared to the experimental data –roughly 100 and 500 respectively– we expect that particles with the same Stokes number will be driven by fluid velocity fluctuations which are characterized by different values of the residual anisotropy (Casciola *et al.*, 2007). In this context, the shear parameter S^*, which measures the extension of the range of scales where

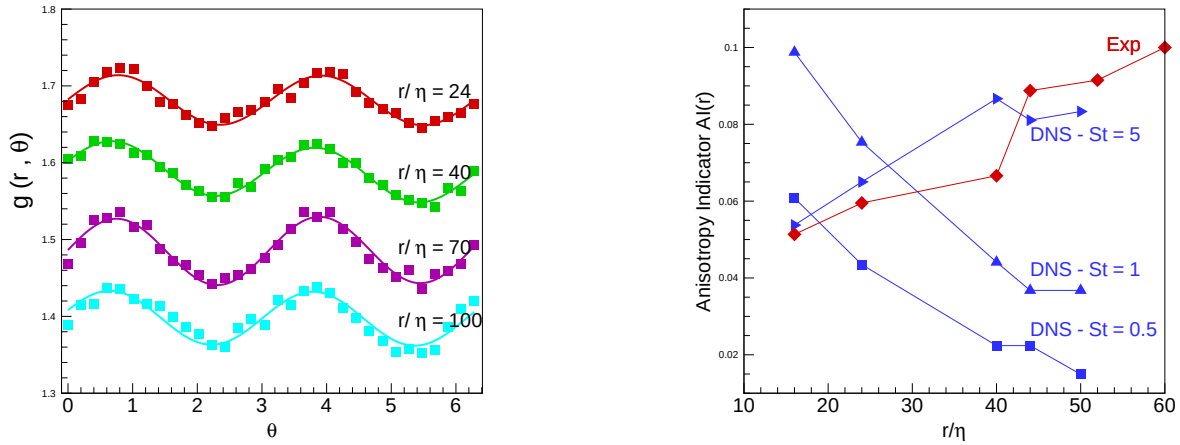

Figure 6. Left panel: the distribution function $\widetilde{g}(r,\theta)$ as a function of θ [Rad] for fixed separation distances, together with its reconstruction by means of the first two angular modes (experimental data). Right panel: the anisotropy indicator $I_A(r)$ computed for both the experimental ($St = 0.3$) and the numerical datasets at different Stokes numbers.

anisotropic effects are relevant, plays also an important role. Direct numerical simulations are run with $S^* = 7$, while the experiments are able to reach only a value $S^* \simeq 4.5$. Hence, we expect that the impact of anisotropy on the characteristics of the clusters is emphasized in the DNS, which is also characterized by a narrower range where isotropy of the velocity field can be recovered.

5. Concluding remarks and perspectives

In this paper, we have explored the issue of particle clustering occurring in presence of large-scale anisotropies which originate from a mean velocity gradient. We have presented preliminary data collected in a novel experimental set-up of a particle-laden homogeneous shear flow, and we have discussed them in comparison with results obtained in a related numerical simulation. Experimental findings are in line with observations from DNS data: the mean flow is able to imprint a preferential orientation of the particle clusters down to the smallest scales. However, in contrast to numerics, which is obviously limited to smaller values of the Reynolds number, the experimental measurements conducted with particles at $St = 0.3$ show a tendency towards isotropy recovery of the clusters orientation, as detected by means of the two-dimensional surrogate of the complete three dimensional angular distribution function. In order to better understand these differences, future work will focus on different issues. In particular, we wish to extend the present experimental dataset, and investigate the effects on the particle distributions associated with changes in both the Stokes number and the size of the particles. We are also currently implementing an optical technique which will give us access to the full three-dimensional particle local concentration field, and plan to combine it with velocity measurement of the carrier fluid in order to explore the onset of two-way coupling at increasing values of the bulk particle concentration.

References

Aliseda, A., Cartellier, A., Hainaux, F. & Lasheras, JC 2002 Effect of preferential concentration on the settling velocity of heavy particles in homogeneous isotropic turbulence.

J. Fluid Mech. **468**, 77–105.

Balachandar, S. & Eaton, J.K. 2010 Turbulent dispersed multiphase flow. *Ann. Rev. Fluid Mech.* **42**, 111–133.

Bec, J., Biferale, L., Cencini, M., Lanotte, A., Musacchio, S. & Toschi, F. 2007 Heavy particle concentration in turbulence at dissipative and inertial scales. *Phys. Rev. Lett.* **98** (8), 84502.

Biferale, L. & Procaccia, I. 2005 Anisotropy in turbulent flows and in turbulent transport. *Physics Reports* **414** (2-3), 43–164.

Casciola, CM, Gualtieri, P., Jacob, B. & Piva, R. 2007 The residual anisotropy at small scales in high shear turbulence. *Phys. Fluids* **19**, 101704.

Crocker, J.C. & Grier, D.G. 1996 Methods of digital video microscopy for colloidal studies. *J. Colloid Interface Sci.* **179** (1), 298–310.

Dunn, W. & Tavoularis, S. 2007 The use of curved screens for generating uniform shear at low reynolds numbers. *Exp. Fluids* **42**, 281–290.

Eaton, J.K. 2009 Two-way coupled turbulence simulations of gas-particle flows using point-particle tracking. *Int. J. Multiphase Flow* **35** (9), 792–800.

Eaton, J. K. & Fessler, J. R. 1994 Preferential concentration of particles by turbulence. *Int. J. Multiphase Flow* **20** (Supplement 1), 169 – 209.

Gualtieri, P., Casciola, C. M., Benzi, R., Amati, G. & Piva, R. 2002 Scaling laws and intermittency in homogeneous shear flow. *Phys. Fluids* **14**, 583.

Gualtieri, P., Picano, F. & Casciola, CM 2009 Anisotropic clustering of inertial particles in homogeneous shear flow. *J. Fluid Mech.* **629**, 25–39.

Jacob, B., Olivieri, A., Miozzi, M., Campana, E.F. & Piva, R. 2010 Drag reduction by microbubbles in a turbulent boundary layer. *Phys. Fluids* **22**, 115104.

Kiger, KT & Pan, C. 2002 Suspension and turbulence modification effects of solid particulates on a horizontal turbulent channel flow. *J. Turbulence* **3** (19), 1–17.

Longmire, E.K. & Eaton, J.K. 1992 Structure of a particle-laden round jet. *J. Fluid Mech.* **236**, 217–257.

Lucci, F., Ferrante, A. & Elghobashi, S. 2010 Modulation of isotropic turbulence by particles of taylor length-scale size. *J. Fluid Mech.* **650**, 5–55.

Maxey, M.R. & Riley, J.J. 1983 Equation of motion for a small rigid sphere in a nonuniform flow. *Phys. Fluids* **26**, 2437.

Poelma, C., Westerweel, J. & Ooms, G. 2007 Particle–fluid interactions in grid-generated turbulence. *J. Fluid Mech.* **589**, 315–351.

Rogallo, R.S. 1981 Numerical experiments in homogeneous turbulence. *Nasa T-M* **81315**.

Squires, K.D. & Eaton, J.K. 1991 Preferential concentration of particles by turbulence. *Phys. Fluids A* **3**, 1169.

Tanaka, T. & Eaton, J.K. 2008 Classification of turbulence modification by dispersed spheres using a novel dimensionless number. *Phys. Rev. Lett.* **101** (11), 114502.

Tsuji, Y., Morikawa, Y. & Shiomi, H. 1984 Ldv measurements of an air-solid two-phase flow in a vertical pipe. *J. Fluid Mech.* **139**, 417–434.

Wang, Lian-Ping & Maxey, Martin R. 1993 Settling velocity and concentration distribution of heavy particles in homogeneous isotropic turbulence. *J. Fluid Mech.* **256**, 27–68.

Yoshimoto, H. & Goto, S. 2007 Self-similar clustering of inertial particles in homogeneous turbulence. *J. Fluid Mech.* **577**, 275–286.